AD-A258 793

②

ARMY RESEARCH LABORATORY

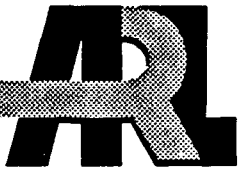

Effects of Surface Structure and of Embedded-Atom Pair Functionals on Adatom Diffusion on FCC Metallic Surfaces

Betsy M. Rice
U.S. ARMY RESEARCH LABORATORY

Cheruvu S. Murthy
IBM SEMICONDUCTOR RESEARCH AND DEVELOPMENT CENTER

Bruce C. Garrett
PACIFIC NORTHWEST LABORATORY

ARL-TR-5 November 1992

DTIC
ELECTE
DEC 16 1992
S D

APPROVED FOR PUBLIC RELEASE; DISTRIBUTION IS UNLIMITED.

92-31470

92

NOTICES

Destroy this report when it is no longer needed. DO NOT return it to the originator.

Additional copies of this report may be obtained from the National Technical Information Service, U.S. Department of Commerce, 5285 Port Royal Road, Springfield, VA 22161.

The findings of this report are not to be construed as an official Department of the Army position, unless so designated by other authorized documents.

The use of trade names or manufacturers' names in this report does not constitute indorsement of any commercial product.

REPORT DOCUMENTATION PAGE

Form Approved
OMB No. 0704-0188

Public reporting burden for this collection of information is estimated to average 1 hour per response, including the time for reviewing instructions, searching existing data sources, gathering and maintaining the data needed, and completing and reviewing the collection of information. Send comments regarding this burden estimate or any other aspect of this collection of information, including suggestions for reducing this burden, to Washington Headquarters Services, Directorate for Information Operations and Reports, 1215 Jefferson Davis Highway, Suite 1204, Arlington, VA 22202-4302, and to the Office of Management and Budget, Paperwork Reduction Project (0704-0188), Washington, DC 20503.

1. AGENCY USE ONLY *(Leave blank)*	2. REPORT DATE	3. REPORT TYPE AND DATES COVERED
	November 1992	Final, July 1988–January 1992

4. TITLE AND SUBTITLE

Effects of Surface Structure and of Embedded-Atom Pair Functionals on Adatom Diffusion on FCC Metallic Surfaces

5. FUNDING NUMBERS

PR: 1L161102AH43

6. AUTHOR(S)

Betsy M. Rice, Cheruvu S. Murthy[†], and Bruce C. Garrett[††]

7. PERFORMING ORGANIZATION NAME(S) AND ADDRESS(ES)

8. PERFORMING ORGANIZATION REPORT NUMBER

9. SPONSORING/MONITORING AGENCY NAME(S) AND ADDRESS(ES)

U.S. Army Research Laboratory
ATTN: AMSRL-OP-CI-B (Tech Lib)
Aberdeen Proving Ground, MD 21005-5066

10. SPONSORING/MONITORING AGENCY REPORT NUMBER

ARL-TR-5

11. SUPPLEMENTARY NOTES

[†] IBM Semiconductor Research and Development Center, Hopewell Junction, NY
[††] Molecular Sciences Research Center, Pacific Northwest Laboratory, Richland, WA
Pacific Northwest Laboratory is operated for the U.S. Dept. of Energy by Battelle Memorial Institute.

12a. DISTRIBUTION/AVAILABILITY STATEMENT

Approved for public release; distribution is unlimited.

12b. DISTRIBUTION CODE

13. ABSTRACT *(Maximum 200 words)*

Rates of self-diffusion on the (100) and (110) surfaces of nickel have been calculated using variational transition state theory (VTST) and four different interatomic potential energy functions based on the embedded-atom method (EAM). Static properties of a single nickel atom on the (111) surface, as well as on the (100) and (110) surfaces, are also presented. The embedded-atom pair functionals consist of effective pairwise additive and many-body cohesive interactions parameterized to the bulk and a few defect properties of nickel. VTST calculations of surface diffusion provide Arrhenius parameters and diffusion coefficients for comparison with experiment and among the four EAM potentials employed. An analysis of the estimated diffusion rates based on hopping mechanism and the four pair functionals reveals that diffusion will occur more readily on (111) surface and that self-diffusion on (110) surface exhibits directional anisotropy. The diffusion rate variation from one pair functional to another is interpreted in terms of the effective pair potentials.

14. SUBJECT TERMS

nickel; embedded-atom-method; surface diffusion; variational transition state theory; diffusion

15. NUMBER OF PAGES
39

16. PRICE CODE

17. SECURITY CLASSIFICATION OF REPORT	18. SECURITY CLASSIFICATION OF THIS PAGE	19. SECURITY CLASSIFICATION OF ABSTRACT	20. LIMITATION OF ABSTRACT
UNCLASSIFIED	UNCLASSIFIED	UNCLASSIFIED	UL

INTENTIONALLY LEFT BLANK.

TABLE OF CONTENTS

Accession For
NTIS GRA&I
DTIC TAB
Unannounced
Justification
By
Distribution/
Availability Codes
Dist | Avail and/or Special
A-1

INTENTIONALLY LEFT BLANK.

LIST OF FIGURES

LIST OF TABLES

INTENTIONALLY LEFT BLANK.

ACKNOWLEDGMENTS

This work was partially supported by the Air Force office of Scientific Research under grant number F49620-88-C-0086. Part of this work was carried out at Chemical Dynamics Corporation and the authors wish to thank Dr. M. J. Redmon for his interest and encouragement. We also wish to thank Drs. A. F. Voter of Los Alamos National Laboratory, Los Alamos, NM, and L. Hansen of the Technical University of Denmark, Lyngby, for providing the preprints of their work prior to publication. In addition, we thank the former and Dr. S. M. Foiles of Sandia National Laboratories, Livermore, CA, for useful correspondence on their EAM models, Dr. P. J. Feibelman of Sandia National Laboratories, Albuquerque, NM, for useful discussions, and Dr. G. R. Srinivasan of IBM, East Fishkill, NY, for useful conversations and general support.

INTENTIONALLY LEFT BLANK.

1. INTRODUCTION

Most processes occurring on a crystal surface and at interfaces are expected to be influenced by the kinetics of the atoms. The mobility of atoms on a crystal surface can be orders of magnitude larger than in the bulk at the same temperature and become the determining step in many processes such as surface reconstruction, chemical reaction, and epitaxial growth. Diffusion on metals continues to receive both experimental and theoretical attention (Ehrlich and Stolt 1980; Doll and Voter 1987; Bonzel 1983; Ehrlich 1990). The relation between the surface diffusivity and surface structure has been studied previously by detailed molecular dynamic (MD) simulations using simple model potential energy functions, which are typically pairwise additive. These studies (De Lorenzi 1986; De Lorenzi and Jacucci 1985) have shown that the surface structure and the softness of the repulsive potential play a dominant role in determining the diffusion properties and that the migration of adatoms can occur not only through simple hops between binding sites on a surface, but through more complicated mechanisms, such as adatom exchange on channelled surfaces. In modelling metallic materials, however, simple pair potentials do not adequately describe the elastic properties of the metal and require a volume-dependent energy term to correct for this inadequacy (Lee 1981; Johnson 1988). Ambiguities arise in defining the termination of the volume at surfaces and bulk defects, thus introducing additional uncertainty into the model.

The embedded atom method (EAM) was recently developed (Daw and Baskes 1983, 1984; Finnis and Sinclair 1981) as a means of calculating realistic ground-state properties of metallic systems, and circumvents the definition of volume by using an energy term which is electron-density-dependent, a property which is always definable. The electron-density-dependent term is the embedding energy, or the energy required to embed an atom into the local electron density of all surrounding atoms. To our knowledge, our analysis of various embedded-atom-type modeling schemes for adatom diffusion studies represents the first study based on the realistic bulk models. The major goal of this study is to examine the use of commonly used EAM potentials, which have been parameterized to reproduce bulk properties in adatom/surface studies, and to determine the applicability of these potential energy functions for studies of interfacial processes. As an initial step towards such studies, self-diffusion on nickel surfaces is chosen as a prototype, but the results can be extended to any face-centered cubic (FCC) system.

For estimating the diffusion coefficients and Arrhenius parameters, we used the variational transition state theory (VTST) approach, instead of adapting the cost-intensive MD simulations, which yield quite detailed information. VTST has been used successfully in calculating rates of gas phase reactions.

Additionally, it has been applied to other gas-surface diffusion studies. We refrained from employing molecular statics due to both the anharmonic features of the potential energy surface and the complicated saddle point surface in configuration space. In the present study, we present results of VTST calculations of diffusion of atomic nickel on several nickel surfaces using four different EAM potential functions. These pair functionals provide similar descriptions of the atomic interaction, but have completely different functional forms for the pairwise interaction as well as for the embedding function and the atomic density.

The remainder of this report is organized as follows: Section 2 provides details of (a) a brief review of the dynamical method, VTST; (b) the background and a short description of the EAM potentials used in this study; and (c) the description of the structural models of the nickel lattices used in the calculations. Discussion of the results of surface self-diffusion and the properties of the nickel adatom on different nickel surfaces are presented in Section 3 and the results are summarized in Section 4.

2. THEORY AND MODELS

2.1 VTST Theory. Surface diffusion is typically thought of as a random walk model of uncorrelated hops of an isolated adatom to equivalent and adjacent binding sites. Each hop is assumed to be an individual unimolecular process with thermal rate constant, k(T). The thermal diffusion coefficient, D(T), can be described in terms of the unimolecular rate constant:

$$D(T) = \frac{a^2}{2\gamma} k(T) \tag{1}$$

where a is the hop length and γ is the dimensionality of the system ($\gamma = 2$ for diffusion on a surface wherein all binding sites are equivalent; and $\gamma = 1$ for surface diffusion along channels [Voter and Doll 1984] such as along the [1$\bar{1}$0] or [001] directions on Ni[1$\bar{1}$0]).

The rate constant k(T) is calculated from canonical VTST with semiclassical adiabatic ground-state transmission coefficients. VTST has been used successfully in calculating such rates in other surface diffusion studies; details are given elsewhere (Truhlar, Isaacson, and Garrett 1983; Lauderdale and Truhlar 1985; Truong and Truhlar 1987, 1988). In review, the procedure consists of first locating the reactant, product, and saddle point geometries (locations at which the gradient vanishes), then determining the reaction path by following the negative of the gradient vector in mass weighted coordinates from the saddle point down into the reactant and product geometries. The reaction coordinate is defined as the distance on the reaction path from the saddle point and, by convention, s is negative on the reactant side

of the saddle point. The generalized transition state theory rate is expressed in terms of the location of the transition state along the reaction coordinate

$$k^{GT}(T,s) = \frac{k_B T}{h} \frac{Q^{GT}(T,s)}{Q^{R}(T)} \exp[-\frac{V_{MEP}(s)}{k_B T}] \quad (2)$$

where k_B is Boltzmann's constant; T is the temperature of the system; Q^{GT} (T, s) is the partition function for the bound degrees of freedom at the generalized transition state location at s; V_{MEP} (s) is the potential along the reaction path; h is Planck's constant; and Q^{R} (T) is the partition function of the reactant species. The partition functions are defined with their zeros of energies at the local minimum of the potential for the bound degrees of freedom, and can be evaluated from the potential energy surface using standard statistical mechanical methods. In canonical variational transition state theory, the location of s is optimized to minimize the rate. Quantum mechanical effects such as tunneling and zero-point energy effects are treated in the VTST calculation; however, these effects are not important in the systems studied. Additionally, variationally optimizing the location of the dividing surface (i.e., the choice of s in Equation 2) always yielded the saddle point (i.e., s = 0).

2.2 Embedded-Atom Pair Functionals. The derivation of the embedded-atom method and its applications to metallic systems are given elsewhere (Daw and Baskes 1983, 1984; Finnis and Sinclair 1981). Its basis on density functional theory, low computational demands, and success in describing bulk phenomena make the method a desirable one for use in computer simulation of interfacial processes in metals.

In the EAM, the energy of a collection of atoms is expressed as a sum of a density-dependent embedding energy and a pair interaction term,

$$U = \sum_i F_i(\rho_i) + \frac{1}{2}\sum_{j \neq i} \Phi_{ij}(r_{ij}) , \quad (3)$$

where F_i (ρ_i) is the energy needed to embed atom i into the local electron density ρ_i of the surrounding atoms, and Φ_{ij} is a pair potential between atoms i and j. The functional form of the EAM has been derived by Manninen (1986) and Jacobsen, Nørskov, and Puska (1987) using density functional theory. The two-body potential within this effective medium theory arises from atomic-core-electron gas

electrostatic attraction whereas it is considered to be repulsive in some of the empirical procedures described below. Further, in some empirical approaches, the two-body potential is separated into a product of two one-atom functionals, analogous to the embedding energy term, while some other EAM-type models have used nonseparable forms. Different empirical schemes have thus been used to construct embedded atom pair functionals for nickel; they are summarized below.

In the Foiles, Baskes, and Daw (FBD) (1986) approach, the local electron density into which atom i is embedded is approximated by the sum over atomic electron densities $\rho^a_j(r_{ij})$ from all other atoms in the system:

$$\rho_i = \sum_j \rho^a_j(r_{ij}) \ . \tag{4}$$

This functional form has the advantage of including many-body interactions due to the nonlinear nature of the embedding function even though the computational effort of evaluating the embedding energy is similar to that for the pairwise-additive interactions. The functional form of the pairwise additive term is:

$$\begin{aligned} \Phi_{ij}(r) &= [Z_i(r)Z_j(r) - Z_i(r_c)Z_j(r_c)]/r \ , & r < r_c \\ &= 0 & r \geq r_c \end{aligned} \tag{5}$$

where $Z_m(r)$ is the effective charge of atom m, and r_c is chosen to be large enough that the pair interactions are very small at that value. The effective charge of an atom is given the functional form as follows:

$$Z(r) = Z_0(1 + \beta r^\nu)\exp(-\alpha r) \ . \tag{6}$$

The atomic densities are approximated by the single-determinant Hartree-Fock calculations of Clementi and Roetti (1974). For nickel, the atomic density is further approximated as the sum of electron densities from the 3d and 4s shells, weighted by the number of electrons in each shell. The number of 4s electrons, n_s, is used as an adjustable parameter and is set to two for all the calculations reported here.

For a given set of parameters for the atomic densities and pair interaction terms, the embedding function was then adjusted (Foiles 1985) so that the simplified equation of state of the metal (Rose, Smith, Guinea, and Ferrante 1984) was exactly reproduced for successive values of the density. The embedding

function for nickel was represented in a tabular form as a function of atomic density. The four parameters appearing in Equation 6 and the embedding function were fitted (Foiles, Baskes, and Daw 1986) to experimental data for the bulk (equation of state, elastic modulii, defect energetics, and heats of solutions of binary alloys) by a least-squares procedure and those defining the pair interactions for nickel are given in Table 1. In the present application, the tabulated embedding function is fitted to a cubic spline.

The differences between the FBD and other EAM approaches are primarily found in the derivation and interpretation of the electron density surrounding the atom and the embedding function. Voter and Chen (VC) (1987) have basically followed the FBD scheme described in Equations 3 and 4, with the following deviations: The pairwise additive interaction is taken to be a Morse potential,

$$\Phi_{ij}(r) = D_M\{1 - \exp[-\alpha_M(r - R_M)]\}^2 - D_M , \tag{7}$$

where R_M, D_M, and α_M define the location, depth, and curvature of the minimum, respectively. The density function $\rho(r)$ is

$$\rho(r) = r^6[\exp(-\beta r) + 2^9\exp(-2\beta r)] , \tag{8}$$

which is a modification of the density of a hydrogenic 4s orbital. The functions $\Phi(r)$ and $\rho(r)$ and the corresponding first derivatives are forced to go smoothly to zero at a cutoff distance, r_c. The four parameters for Equations 7 and 8 at the cutoff r_c and the embedding function were fitted to the same experimental data used in the FBD fit (Table 1). Like the FBD embedding function, the VC embedding function is obtained in terms of tabular form.

Oh and Johnson's (OJ) (1988) approach was to develop an EAM model with simple functional forms which result in fewer parameters to fit and thus provide easy access for adapting the EAM model. The embedding energy $F(\rho)$ is defined as

$$F(\rho) = \alpha(\rho_i/\rho_e)^n + b(\rho_i/\rho_e) , \tag{9}$$

where

$$\rho_i(r) = \sum_{j \neq i} f(r) , \tag{10}$$

Table 1. Parameters for the EAM Potentials

FBD Potential		VC Potential	
Z_0 (eV–Å)$^{-1/2}$	37.9326	D_M (eV)	1.5335
α (Å^{-1})	1.8633	α_M (Å^{-1})	1.7728
β (Å$^{-\nu}$)	0.8957	β_M (Å^{-1})	2.2053
ν	1	R_M (Å)	3.6408
N_S	2	r_{cut} (Å)	4.7895
r_{cut} (Å)	4.8		
OJ Potential[a]		**ATVF Potential[b]**	
β	6	a_1	29.057085
γ	9	a_2	–76.04625
δ	20	a_3	48.08920
r_{cut}	1.9	a_4	–25.96604
f_e	1.0	a_5	79.15121
ϕ_e	0.63199	r_1	1.2247449
a	–3.1684	r_2	1.1547054
b	–5.1237	r_3	1.1180065
n	0.12501	r_4	1.0000000
ρ_e	12.551	r_5	0.8660254
—	—	A_1	60.537985
—	—	A_2	–80.102414
—	—	R_1	1.2247449
—	—	R_2	1.1180065

[a] ϕ_e and r_{cut} are expressed in eV and nearest neighbor distance $\frac{3.52}{\sqrt{2}}$ Å, respectively. The other parameters are dimensionless.

[b] The coefficients are in units of eV and the lattice parameter, 3.52 Å, respectively.

and

$$f(r) = f_e \exp(-\beta[r/r_e - 1]) - f_e \exp(-\beta[r_c/r_e - 1])$$
$$- \beta f_e \{1 - \exp(\delta[r/r_e - r_c/r_e])\} \exp(-\beta[r_c/r_e - 1])/\delta . \quad (11)$$

The pairwise additive interaction has a similar form

$$\Phi(r) = \Phi_e \exp(-\gamma[r/r_e - 1]) - \Phi_e \exp(-\gamma[r_c/r_e - 1])$$
$$-\gamma\Phi_e \{1 - \exp(\delta[r/r_e - r_c/r_e])\} \exp(-\gamma[r_c/r_e - 1])/\delta . \quad (12)$$

The nine parameters for both embedding and pair potential terms (Equations 9–12) are given in Table 1.

Ackland, Tichy, Vitek, and Finnis (ATVF) (1987) identified $F(\rho)$ with the second moment of the density of states and thus used a square-root function for $F(\rho)$. The function for both $F(\rho)$ and Φ consist of a series expansion with built-in step functions (denoted H(x) in Equation 17), the coefficients of which have been fitted to the experimental data as well as the pressure-volume values calculated from first-principles. The forms of the functions are as follows:

$$F(\rho_i) = -\sqrt{\rho_i} , \quad (13)$$

where

$$\rho_i = \sum_{j \neq i} \phi(r_{ij}) \quad (14)$$

and

$$\phi(r) = \sum_{k=1}^{2} \{A_k (R_k - r)^3 H(R_k - r)\} . \quad (15)$$

The pairwise additive term Φ has the form

$$\Phi(r) = \sum_{k=1}^{5} \{a_k (r_k - r)^3 H(r_k - r)\} . \quad (16)$$

The step function H(x) used in Equations 15 and 16 has the form

$$H(x) = 0, \quad x < 0$$
$$= 1, \quad x \geq 0. \tag{17}$$

The 14 parameters which include the embedding energy term for the ATVF potential energy function are given in Table 1.

2.3 Lattice Models. The structural model used in self-diffusion on Ni(100) consists of 162 atoms over 4 layers; 41 atoms are in each of the first and third layers, and 40 atoms are in each of the second and fourth layers. Figure 1a illustrates the crystal model used in this calculation; the six shaded atoms denote the first-layer atoms which were allowed to move in this calculation. The reactant and product sites are labelled R and P, respectively, and lie over the two second-layer atoms which were allowed to move in this calculation. The transition state, which is located directly between the reactant and product sites, is labelled T.

The model of the Ni(111) crystal consists of 120 nickel atoms with 4 layers. There are 27 atoms in the first and fourth layers, and 33 atoms in the second and third layers. Figure 1b illustrates the model used in this calculation, and the reactant, product, and transition state sites are labelled R, P, and T, respectively. Four surface atoms (shaded in the figure) and three second-layer atoms surrounding the reactant site were allowed to move.

Two different models were used in the Ni(110) calculations, because there are two different diffusional directions; one along the [1$\bar{1}$0] direction (parallel to the channel) and the other along the [001] direction (perpendicular to the channel). The model for calculation of diffusion in the [1$\bar{1}$0] direction consists of 186 atoms over 5 layers and is illustrated in Figure 1c. There are 42 atoms in the first, third, and fifth layers, and 30 atoms in the second and fourth layers. Six surface atoms (darkly shaded) and four second-layer atoms (lightly shaded) adjacent to the labelled reactant, product, and transition state sites were allowed to move. The model for calculation of diffusion in the [001] direction (Figure 1d,) has 219 atoms, with 49 atoms in each of the first, third, and fifth layers; and 36 atoms in each of the second and fourth layers. Atoms (six in the first layer and four in the second layer) adjacent to reactant, product, and transition state sites (labelled R, P, and T, respectively) were allowed to move and are shaded.

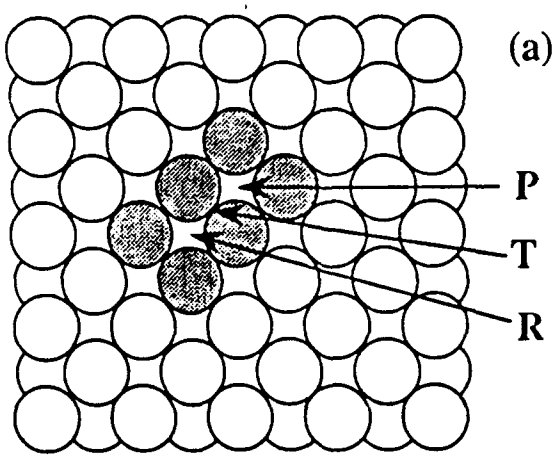

Figure 1a. Ni(100).

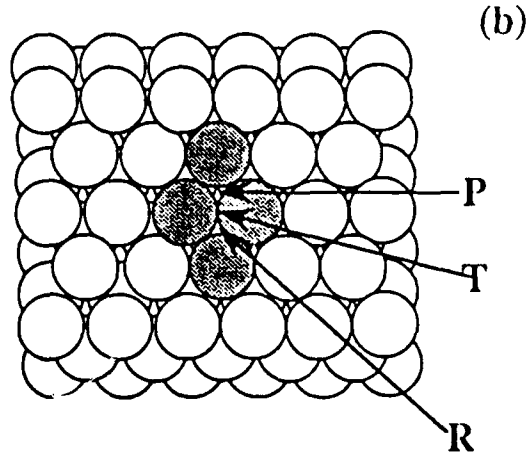

Figure 1b. Ni(111).

Crystal Lattice Models Used in the Calculations of a Nickel Adsorbate

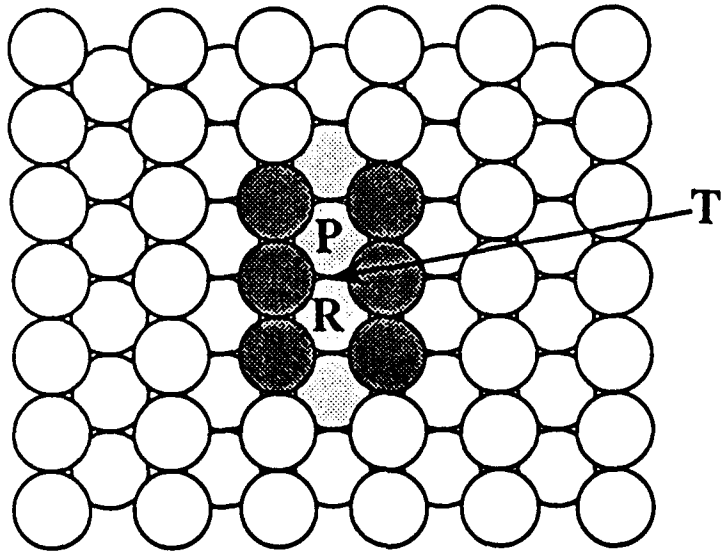

Figure 1c. Crystal Lattice Models Used in the Calculations of a Nickel Adsorbate on Ni(110) (for calculations of diffusion in the [1$\bar{1}$0] direction)

The number of atoms allowed to move in any of the crystal models studied was not varied to check for convergence of a diffusion rate. The substrate models were arbitrarily chosen and used in each calculation for comparative purposes only. However, identical lattice models were used for all the

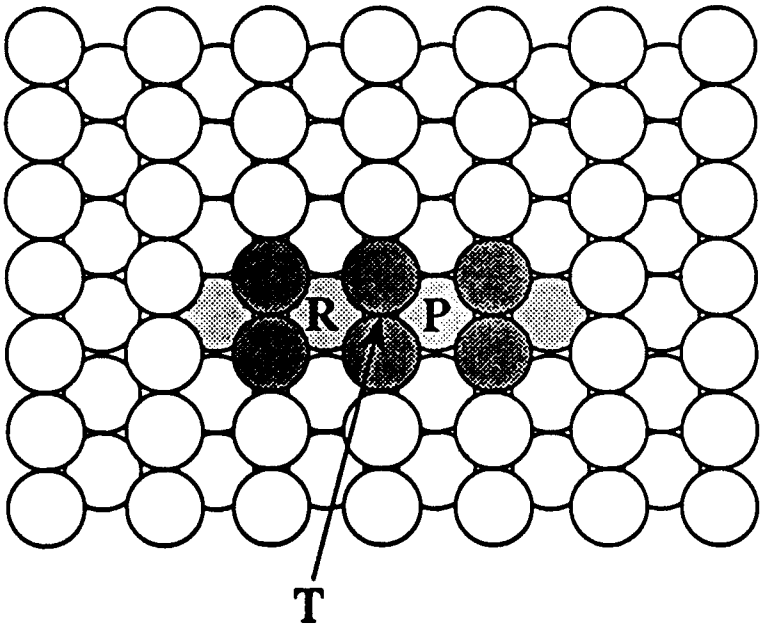

Figure 1d. Crystal Lattice Models Used in the Calculations of a Nickel Adsorbate on Ni(110) (for calculations of diffusion in the [001] direction).

potential models because our interest was not in calculating the absolute true rate, because of the lack of consistent experimental data with which to compare, but rather to investigate how the potentials compared to each other. Indeed, for estimating a very precise diffusion rate, it may be necessary to allow for more substrate atoms to relax because of the coupling between the diffusing Ni atom and the Ni-substrate atom motion. However, in conjunction with the results available in the research literature, which is discussed in Section 3.3.1, the calculated rates may not vary significantly when more substrate atoms are allowed to move.

3. RESULTS AND DISCUSSION

Diffusion coefficients for self-diffusion of nickel on the (100) and (110) surfaces are given in Table 2; Arrhenius parameters are extracted from linear least-squares fits of ln [D(T)] over the temperature ranges listed in Table 2 and are given in Table 3, along with reported experimental values. The tabulated diffusion coefficients as a function of temperature are provided to reflect on the accuracy of fit to Arrhenius form over a temperature range when required.

3.1 Surface Structure Effects. Comparison of the classical diffusional barriers for Ni/Ni(100), Ni/Ni(110), and Ni/Ni(111) indicates that diffusion will occur most readily on the (111) surface, and more readily along the channels of atoms on the Ni(110) surface, which is typical of the FCC metals (Ehrlich

Table 2. Calculated Diffusion Coefficients (cm^2/s)

T(K)	FBD[a]	VC[b]	OJ[c]	ATVF[d]
Ni/Ni(100)				
50.0	1.286 (–67)	6.454 (–74)	2.101 (–48)	2.286 (–96)
100.0	1.786 (–35)	1.270 (–38)	7.185 (–26)	8.863 (–50)
200.0	2.463 (–19)	6.706 (–21)	1.545 (–14)	2.254 (–26)
223.0	1.145 (–17)	4.548 (–19)	2.295 (–13)	5.931 (–24)
243.0	1.789 (–16)	9.308 (–18)	1.584 (–12)	3.207 (–22)
263.0	1.840 (–15)	1.204 (–16)	8.154 (–12)	9.464 (–21)
283.0	1.362 (–14)	1.086 (–15)	3.331 (–11)	1.732 (–19)
300.0	6.054 (–14)	5.589 (–15)	9.510 (–11)	1.513 (–18)
400.0	3.014 (–11)	5.129 (–12)	7.500 (–09)	1.255 (–14)
600.0	1.504 (–08)	4.724 (–09)	5.936 (–07)	1.050 (–10)
1000.0	2.170 (–06)	1.113 (–06)	1.965 (–05)	1.452 (–07)
1100.0	4.276 (–06)	2.346 (–06)	3.167 (–05)	3.893 (–07)
1200.0	7.524 (–06)	4.364 (–06)	4.714 (–05)	8.860 (–07)
1300.0	1.214 (–05)	7.381 (–06)	6.601 (–05)	1.777 (–06)
1400.0	1.829 (–05)	1.158 (–05)	8.809 (–05)	3.226 (–06)
1500.0	2.609 (–05)	1.711 (–05)	1.131 (–04)	5.410 (–06)
1600.0	3.560 (–05)	2.407 (–05)	1.408 (–04)	8.504 (–06)
Ni/Ni(110)[1$\bar{1}$0]				
50.0	7.276 (–54)	1.711 (–56)	2.592 (–47)	3.587 (–68)
60.0	1.628 (–45)	1.062 (–47)	4.720 (–40)	1.971 (–57)
80.0	4.712 (–35)	1.107 (–36)	5.953 (–31)	5.580 (–44)
100.0	9.263 (–29)	4.714 (–30)	1.788 (–25)	6.871 (–36)
125.0	1.027 (–23)	9.723 (–25)	4.417 (–21)	2.101 (–29)
150.0	2.394 (–20)	3.435 (–21)	3.791 (–18)	4.500 (–25)
200.0	3.917 (–16)	9.465 (–17)	1.783 (–14)	1.190 (–19)

Note: Power of 10 in parenthesis.

[a]Foiles, Baskes, and Daw approach
[b]Voter and Chen approach
[c]Oh and Johnson approach
[d]Ackland, Tichy, Vitek, and Finnis approach

Table 2. Calculated Diffusion Coefficients (cm^2/s) (continued)

T(K)	FBD[a]	VC[b]	OJ[c]	ATVF[d]
250.0	1.327 (–13)	4.387 (–14)	2.865 (–12)	2.159 (–16)
300.0	6.459 (–12)	2.631 (–12)	8.489 (–11)	3.227 (–14)
400.0	8.308 (–10)	4.393 (–10)	5.880 (–09)	1.696 (–11)
500.0	1.532 (–08)	9.471 (–09)	7.485 (–08)	7.299 (–10)
600.0	1.069 (–07)	7.337 (–08)	4.082 (–07)	8.975 (–09)
1,100.0	8.844 (–06)	7.689 (–06)	1.930 (–05)	2.701 (–06)
1,200.0	1.375 (–05)	1.213 (–05)	2.838 (–05)	4.780 (–06)
1,300.0	1.998 (–05)	1.799 (–05)	3.934 (–05)	7.750 (–06)
1,400.0	2.753 (–05)	2.521 (–05)	5.204 (–05)	1.173 (–05)
1,500.0	3.633 (–05)	3.377 (–05)	6.633 (–05)	1.679 (–05)
1,600.0	4.632 (–05)	4.362 (–05)	8.201 (–05)	2.299 (–05)
Ni/Ni(110) [001]				
50.0	2.992 (–134)	3.346 (–171)	1.387 (–104)	8.352 (–157)
60.0	2.122 (–112)	3.420 (–143)	1.141 (–87)	3.460 (–131)
80.0	4.611 (–85)	3.731 (–108)	1.689 (–66)	3.876 (–99)
100.0	1.209 (–68)	4.103 (–87)	8.891 (–54)	6.897 (–80)
125.0	1.690 (–55)	2.875 (–70)	1.378 (–43)	1.794 (–64)
150.0	9.932 (–47)	4.964 (–59)	8.715 (–37)	3.461 (–54)
200.0	9.228 (–36)	5.629 (–45)	2.826 (–28)	2.554 (–41)
250.0	3.543 (–29)	1.541 (–36)	3.658 (–23)	1.364 (–33)
300.0	8.716 (–25)	6.522 (–31)	9.412 (–20)	1.947 (–28)
400.0	2.695 (–19)	7.078 (–24)	1.736 (–15)	5.100 (–22)
500.0	5.166 (–16)	1.181 (–19)	3.215 (–13)	2.913 (–18)
600.0	6.531 (–14)	7.723 (–17)	1.426 (–11)	8.932 (–16)

Note: Power of 10 in parentheses.

[a]Foiles, Baskes, and Daw approach
[b]Voter and Chen approach
[c]Oh and Johnson approach
[d]Ackland, Tichy, Vitek and Finnis approach

Table 3. Arrhenius Parameters and Static Properties

	Theoretical				Experimental			
					FIM		Mass Transfer	
	FBD[a]	VC[b]	OJ[c]	ATVF[d]	Tung & Graham (1980)	Liu et al.[e] (1991)	Bonzel & Latta (1978)	Maiya & Blakely (1965)
Ni/Ni(100)								
E_a (eV)	0.64	0.70	0.45	0.93	0.63	—	—	1.54
D_0 (cm^2/s)	0.0035	0.0037	0.0035	0.0064	—	—	—	2.6
$V^\dagger$ (eV)[f]	0.64	0.71	0.45	0.94	—	—	—	—
Δz (Å)[g]	1.87	1.83	2.00	1.93	—	—	—	—
Ni/Ni(110)[1$\bar{1}$0]								
E_a (eV)	0.50	0.53	0.44	0.64	0.23	0.45	0.76	1.85
D_0 (cm^2/s)	0.0033	0.0038	0.0036	0.0045	10^{-9}	0.001	0.009	23.9
$V^\dagger$ (eV)[f]	0.50	0.53	0.44	0.65	—	—	—	—
Δz (Å)[g]	1.11	1.06	1.20	1.14	—	—	—	—
Ni/Ni(110)[001]								
E_a (eV)	1.30	1.67	1.01	1.53	0.32	0.45	1.95	1.74
D_0 (cm^2/s)	0.0065	0.0075	0.0065	0.0077	10^{-7}	0.001	470.0	12.8
$V^\dagger$ (eV)[f]	1.31	1.68	1.02	1.54	—	—	—	—
Δz (Å)[g]	1.11	1.06	1.20	1.14	—	—	—	—
Ni/Ni(111)								
E_a (eV)	—	—	—	—	0.33	—	—	—
D_0 (cm^2/s)	—	—	—	—	—	—	—	—
$V^\dagger$ (eV)[f]	0.06	0.07	0.05	0.05	—	—	—	—
Δz (Å)[g]	1.84	1.79	1.94	1.89	—	—	—	—

[a]Foiles, Baskes, and Daw approach
[b]Voter and Chen approach
[c]Oh and Johnson approach
[d]Achland, Tichy, Vitek, and Finnis approach
[e]Reanalyzed data of Tung and Graham (1980) (see text)
[f]Classical diffusional barrier
[g]Distance above the surface in the reactant binding site

and Stolt 1980; Doll and Voter 1987; Bonzel 1983; Ehrlich 1990; De Lorenzi 1986; De Lorenzi and Jacucci 1985). Additionally, all of the models indicate two distinct binding sites on the (111) surface, which was observed in experiment (Tung and Graham 1980). Recent lattice statics calculations (Liu, Cohen, Adams, and Voter 1991) for all the EAM-type FCC metals have led to similar results.

The variations in diffusion rates have been explained in terms of the influence of atomic packing in the different surface structures. The FCC (100) surface is loosely packed compared to the more compact (111) surface. Similarly, in the $[1\bar{1}0]$ direction, the atomic structure of the (110) surface is more compact relative to that in the [001] direction. Detailed MD studies (De Lorenzi, Jacucci, and Pontikis 1982), using Lennard-Jones interatomic potentials for surfaces of rare gas solids, have shown clearly that close packing enhances adatom mobility. Our results, together with the recent calculations (Liu, Cohen, Adams, and Voter 1991) for the FCC metals described by EAM models, confirm these findings. Further details of surface structure effects and the pertinent adatom diffusion mechanisms are discussed in Section 3.3.

3.2 Embedded-Atom Functional Effects. Comparison of diffusion rates among the four EAM potential energy models shows that in all cases, the OJ model predicts the fastest diffusion rates, followed by the FBD model. The VC model predicts a faster diffusion rate than the ATVF model for diffusion on the (100) surface and in the $[1\bar{1}0]$ direction on the (110) surface, but the ordering of diffusion rates is switched for diffusion in the [001] direction on the (110) surface. Dependence of atom diffusion rates on the pair functionals has not been analyzed to date. In order to analyze the different diffusion rates based on different EAM models, we first examined the component terms; such as $\rho(r)$, $F(\rho)$, and $\Phi(r)$, that constitute an embedded-atom pair functional. Furthermore, such an examination is useful in its own right because of the different functional forms and of the empirical procedures employed in devising the various EAM models as discussed briefly in Section 2.2.

The electron density variation, $\rho(r)$, in the modeled nickel is characterized differently in each of the adapted pair functionals. The electron density is a simple superposition of contributions from neighboring atoms. In order to facilitate a suitable comparison of $\rho(r)$ and the resulting $F(\rho)$ of the different EAM models, $\rho(r)$ is scaled to its equilibrium value, ρ_e, the electron density of an atom in the bulk metal at equilibrium. Such a normalized $\rho(r)$ for all the used EAM models is shown in Figure 2. Excepting for the ATVF model, all the other functionals show exponential behavior. The equilibrium electron densities are 0.067, 0.38, 12.55, and 37.41 $Å^{-3}$ for FBD, VC, OJ, and ATVF models, respectively. The large

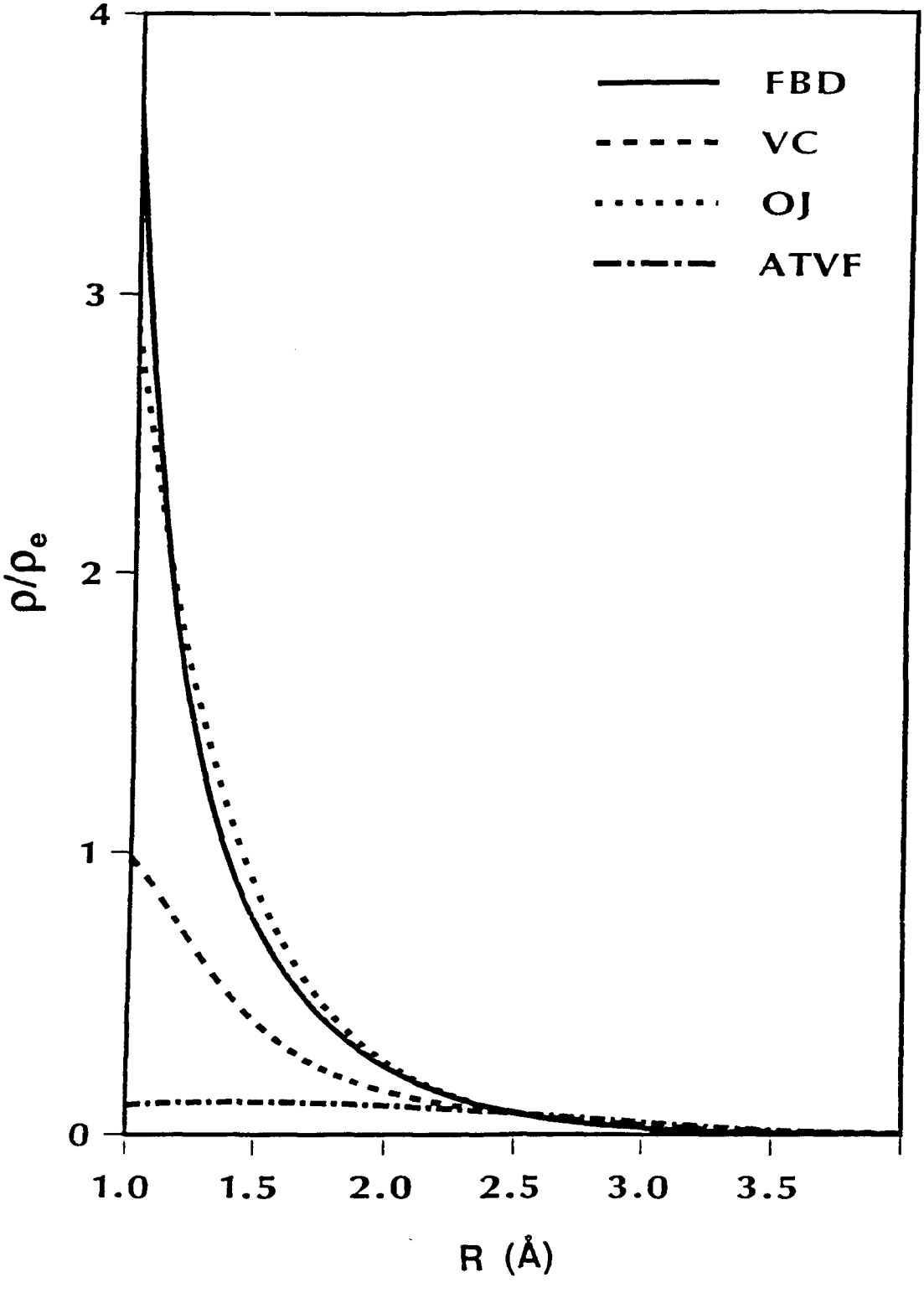

Figure 2. Normalized Electron Density Plots for Nickel as a Function of Interatomic Distance; ρ_e is the Atomic Electron Density in the Bulk Metal at Equilibrium.

differences in ρ_e and $\rho(r)$ are due to the different procedures used for mimicking the solid-state bulk metal atom effects.

The embedding functions based on the respective $\rho(r)$'s are shown in Figure 3. Excepting for the VC model, for which the pair potential is taken to be of Morse type, the other embedding function shapes are similar and the functions are attractive in nature as the corresponding pair interactions are treated to be repulsive. Comparison of diffusion rates based on VC model with that obtained by using other EAM models indicate that the two-body potential can be attractive or repulsive, with the corresponding embedding function being repulsive or attractive, respectively, without much effect on calculated diffusion rates. This may be reasoned out as due to the following: the recipe of fitting to the equation of state brings about some kind of balance between the two terms. Furthermore, the function $F(\rho)$ and $\Phi(r)$ need not be uniquely determined, as discussed by Daw and Baskes (1983) on EAM approach, by the empirical procedures. As the examination of the component terms, $F(\rho)$ and $\Phi(r)$, did not lead to a physically plausible explanation for the variation in diffusion rates based on the different EAM models, the next step we chose was to examine the effective two- and three-body potentials that can be constructed from an EAM model.

Based on detailed MD studies of surface diffusion on FCC and body-centered cubic (BCC) systems, Jacucci and coworkers have shown that the rate of diffusion is expected to be affected by the degree of stiffness in the repulsive wall (De Lorenzi and Jacucci 1985). To investigate this, following Foiles (1985, 1987), we approximated the EAM energy as an effective pair potential by expanding the embedding functional in a Taylor series and dropping three-body and higher order terms. We have thus calculated the effective pair potential $\Phi_{eff}(r)$ as

$$\Phi_{eff}(r) = \Phi(r) + 2F'(\rho_e)\rho(r) + F''(\rho_e)[\rho(r)]^2 \qquad (18)$$

as a function of interatomic distance r for each of the four EAM potential functions described above and show the effective potentials in Figure 4. $F'(\rho_e)$ and $F''(\rho_e)$ in Equation 18 are the first and second derivatives of the embedding energy with respect to the local electron density, ρ.

The effective pair potential curve for the ATVF model differs from the other curves for the FBD, VC, and OJ models both in the repulsive wall region (located at a smaller R/a value) and at R/a values

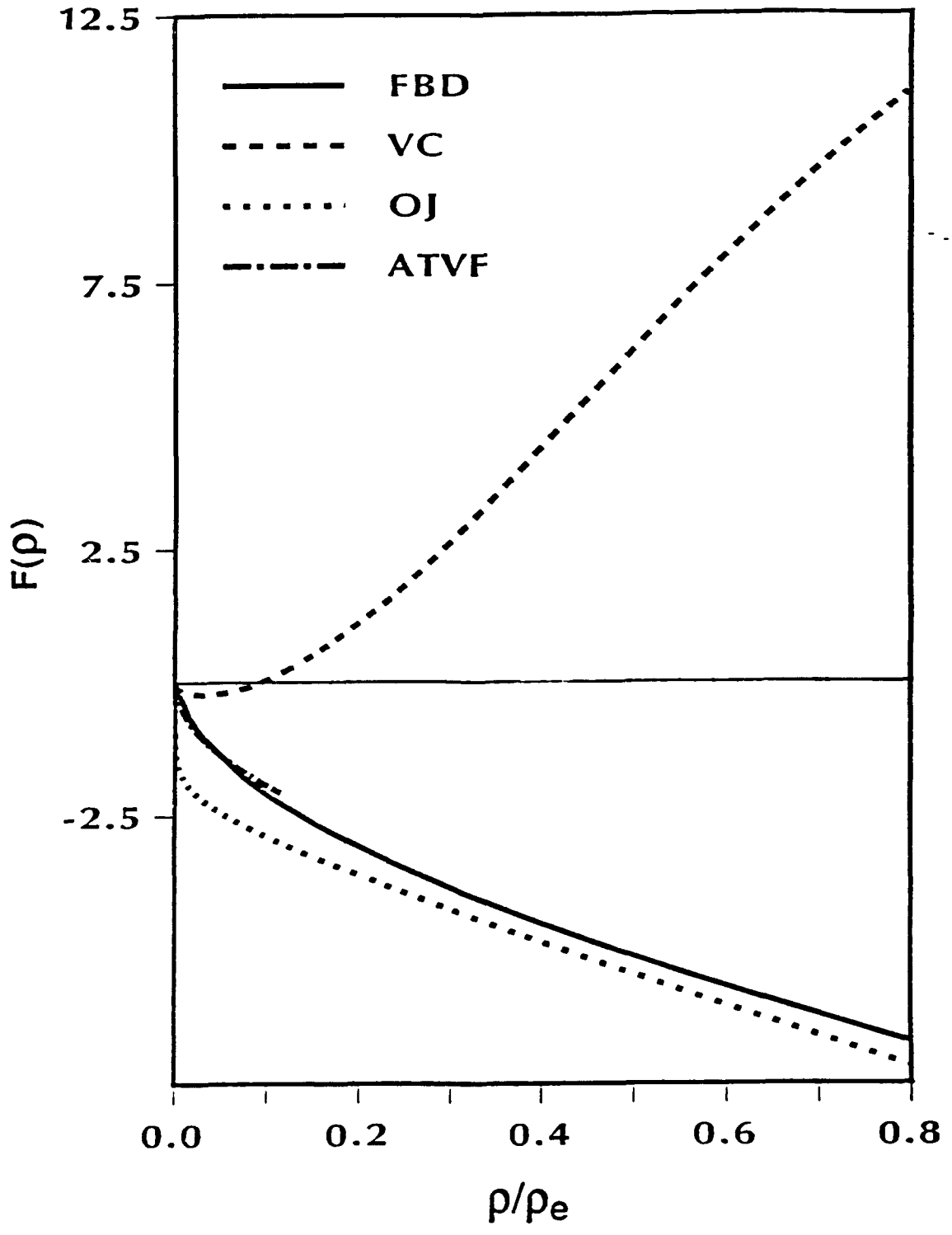

Figure 3. Embedding Function in eV for Nickel as a Function of Normalized Electron Density; ρ_e is the Atomic Electron Density in the Bulk Metal at Equilibrium.

greater than the minimum of the well where a "bump" exists rather than merely an attractive tail. However, on the basis of simulations on self- and defect-diffusion studies in bulk and in grain boundaries, one may safely conclude that the tail region effects are small for adatom diffusion. Although the ATVF potential energy curve has a well depth approximately equal to the OJ curve, its repulsive wall is much softer than the other effective pair potentials. From Table 3 and Figure 5, we find that the ATVF model consistently predicts larger barriers for diffusion (correspondingly lower diffusivities) on the (100) surface and in the $[1\bar{1}0]$ direction on the (110) surface. The predicted large diffusion barriers predicted by the ATVF model thus concur with the conclusion from the detailed MD studies (De Lorenzi and Jacucci 1985) that softness hinders adatom mobility.

The effective potential energy curves for the FBD, VC, and OJ models have a similar shape; the main differences occur in the potential well depth and in the long-range attractive tails. While OJ and FBD curves are superimposable up to the well depth, compared to OJ and FBD curves, the VC curve differs from the repulsive region itself. Of the three effective potentials which have the same shape, the OJ potential energy curve has the deepest attractive well, and the FBD curve has the next deepest well. The activation energies in Table 3 and the Arrhenius plots in Figure 5 indicate that the diffusion rates predicted by these models are also in the same order in terms of fastest to slowest and low to high with respect to barrier height.

Effect of higher-order terms in the Taylor series of $F(\rho)$ on $\Phi_{eff}(r)$ is evident from a comparison with the inset in Figure 2, which corresponds to the $\Phi_{eff}(r)$ computed from only the first two terms in Equation 18. Furthermore, the inclusion of three-body interactions, which is more cumbersome to evaluate, and higher-order terms may lead to a more definitive analysis, in terms of the effective potentials, for the diffusion rates predicted by FBD, VC, and OJ models.

3.3 Comparison With Experiment. Experimental results presented are from FIM and mass transfer experiments; however, the results shown in Table 3 indicate that contradictory experimental data for self-diffusion on nickel exist. Therefore, stringent comparison of the predicted result to experiment is difficult due to the wide variation of experimental results shown in Table 3. FIM measurements provide rates of intrinsic diffusion, and are essentially independent of surface defects, while mass transfer measurements are performed over larger distances on the crystal, thus involving a range of orientations and surface defects. The rates of diffusion in our calculations would, therefore, most likely correspond to the intrinsic diffusion rates measured by FIM.

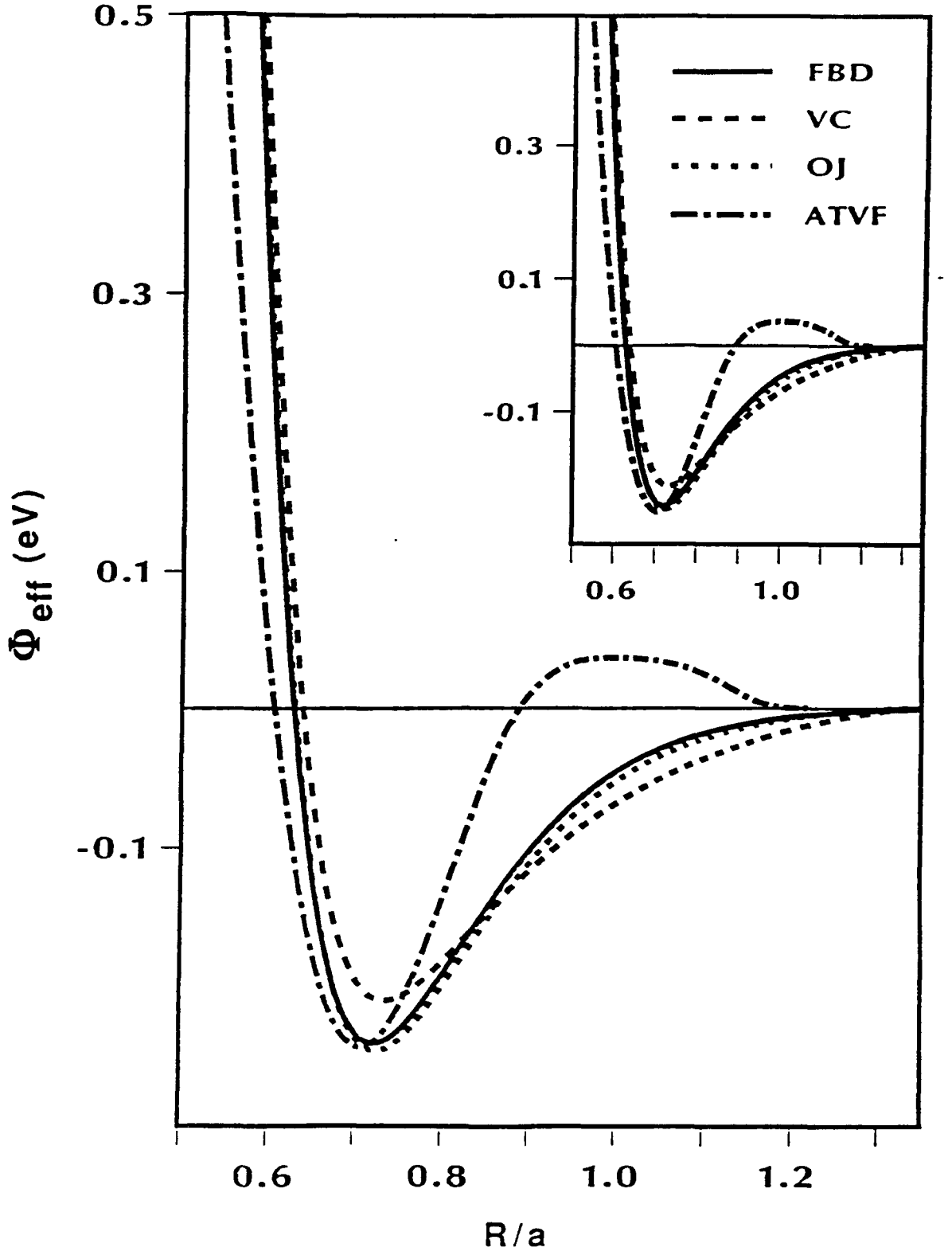

Note: The inset is for the effective pair potential obtained by neglecting second- and higher-order terms in the Taylor expansion of embedding function.

Figure 4. Effective Pair Potential Energy Curves as a Function of Interatomic Distance Scaled to the Lattice Parameter of Nickel, 3.52 Å.

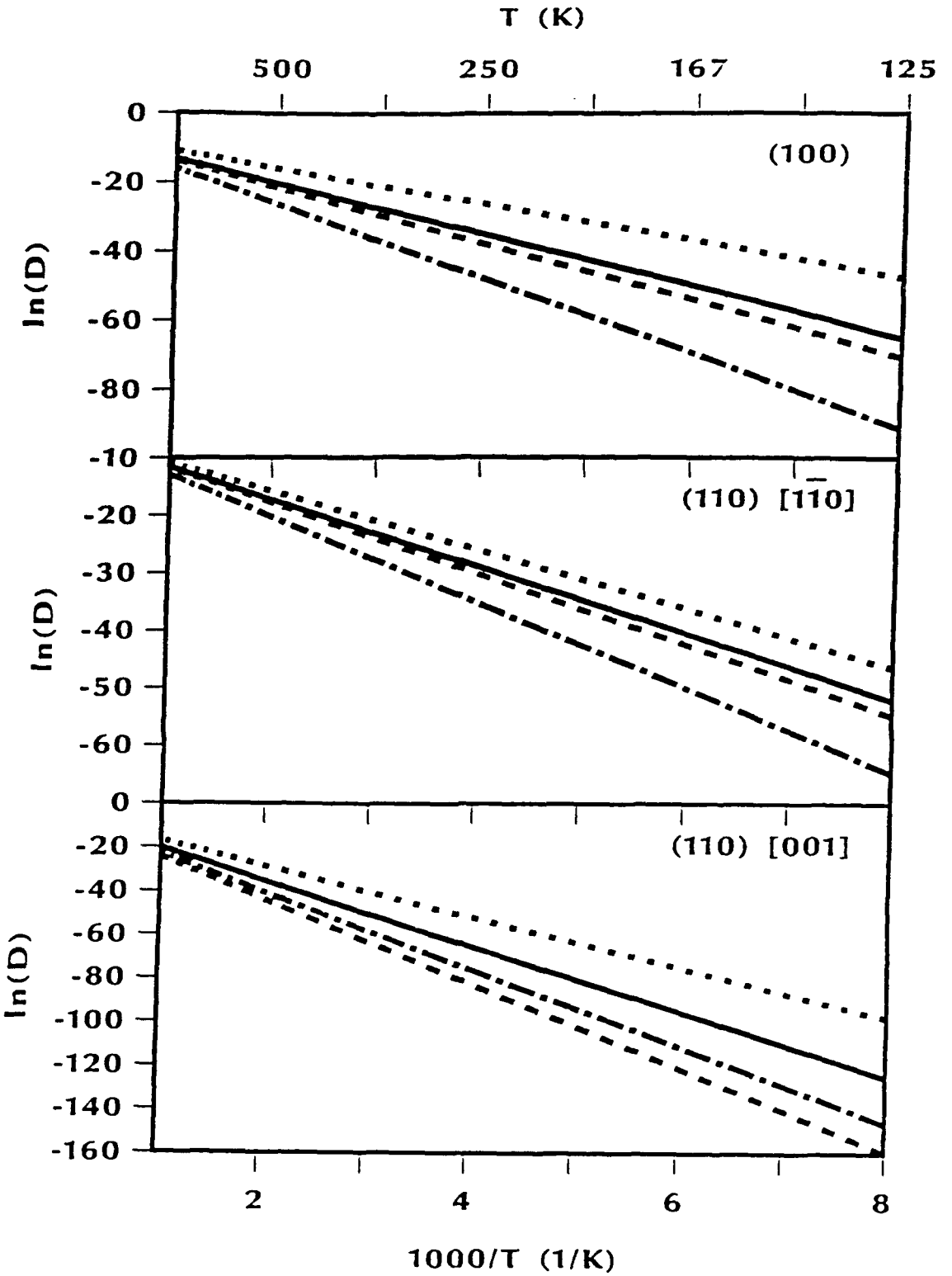

Figure 5. Arrhenius Plot of Self-Diffusion on (100) Surface and on (110) Surface in the Directions of [1$\bar{1}$0] and [001]: (solid line) FBD, (long-dashed line) VC, (short-dashed line) OJ, and (dot-dashed line) ATVF model predictions.

3.3.1 The (100) Surface. Tung and Graham (1980), in a discussion of their FIM results, indicate that while reliable diffusion measurements for the two-dimensional (100) and (111) surfaces are difficult to obtain, the onset temperature for adatom mobility on these surfaces can be accurately determined. By determining the onset temperature, assigning a value of $D = 10^{-17}$ cm^2/s at the onset temperature, and assuming a preexponential factor of

$$\frac{k_B T l^2}{2h}, \tag{19}$$

where l denotes the hop length between binding sites, Tung and Graham (1980) estimate activation energies of 0.63 and 0.33 eV for self-diffusion on the (100) and (111) surfaces, respectively. If the assumptions made by Tung and Graham (1980) are reasonable, all models are in good agreement with experiment for diffusion on the (100) surface, but agreement is poor for the Ni(111) surface. Recent lattice statics calculations (Liu, Cohen, Adams, and Voter 1991) using the VC and another set (Adams, Foiles, and Wolfer 1989) of FBD-type models have led to values of 0.68 and 0.63 eV for the activation energy of self-diffusion on (100) surface. These are in good agreement with our estimated values of 0.71 and 0.64 eV for the VC and FBD models, respectively. The respective preexponential factors, D_0, 5.4, and 1.6 10^{-3} cm^2/s are comparable to our values, 3.7 and 3.5 10^{-3} cm^2/s. These results are based on the hopping mechanism. Discussion involving energetics for more complicated mechanisms such as adatom exchange (Bassett and Webber 1978; Halicioglu and Pound 1979) is included in Section 3.3.3.

The agreement for the energetics based on hopping mechanism between Liu, Cohen, Adams, and Voter's (1991) approach and our VTST calculations (which allowed only a small number of the substrate atoms to move) is remarkable and indicates that the convergence of our estimated diffusion rates is more than adequate for the present comparative studies of potential model effects. The results of these potential-based studies are also in accord with the recent first-principles calculations (Feibelman 1990) of self-diffusion of Al on Al(001). The latter studies have discussed that the atomic relaxations in Al have a small effect on the adatom diffusion barrier height. Liu, Cohen, Adams and Voter (1991) found that typically two to six moving atom layers resulted in activation energy convergence to less than 0.01 eV. These results in conjunction with ours would imply that self-diffusion on the relaxed surface would be slightly different from a rigid substrate and that effects of surface motion on rates would be minimal.

3.3.2 The (111) Surface. The reliability of the estimated activation energy of 0.33 eV for self-diffusion on the (111) surface is questionable due to the existence of two distinct binding sites on this

surface, and the inability of Tung and Graham (1980) to determine the onset temperature for adatom displacement between the two sites. The onset temperature used for the estimate of the activation energy for diffusion on the (111) surface corresponds to movements of adatoms over approximately two lattice spacings, and does not correspond to motion from the two binding sites shown in Figure 1b. All of the four EAM potentials predict two distinct binding sites (denoted in Figure 1b as R and P) in good agreement with experiment (Tung and Graham 1980), but the differences in energies for the two binding sites are less than 0.03 eV for all four potentials, and the barriers to diffusion between the two sites are no greater than 0.07 eV for all four EAM potentials (see Table 3). Rates of self-diffusion on Ni(111) were not calculated because when barriers are too low, the approximation of uncorrelated hops assumed in Equation 1 becomes invalid and other approaches for calculating diffusion coefficients are needed.

3.3.3 The (110) Surface and Diffusion Anisotropy. Comparison of the calculated diffusion rates with experimental values on the Ni(110) surface is also not straightforward because the experimental results are questionable (Bonzel 1983). The data provided by Tung and Graham (1980) for diffusion in the $[1\bar{1}0]$ direction indicate an activation energy of 0.23 eV and an extremely small preexponential factor. Rates of diffusion measured from FIM experiments typically tend to be much larger than those measured from mass transfer methods (by at least 10^3) (Bonzel 1983). The FIM data for Ni(110) presented by Tung and Graham (1980), however, appear to be at least 10^4 smaller than the corresponding mass transfer measurement, in contradiction to typical comparisons of FIM (Tung and Graham 1980) results to mass transfer results (Bonzel and Latta 1978; Maiya and Blakely 1965). This has led Bonzel (1983) in his review of nickel self-diffusion results to question the reliability of the FIM measurements for clean nickel. Recently, Liu, Cohen, Adams, and Voter (1991), in connection with their calculations of surface diffusion based on EAM models, have expressed some concern about fitting an Arrhenius form to a few FIM data points and the resulting large errors in estimates of D_0. Both our estimates, as well as their estimates, are about 10^{-3} cm^2/s compared to the value of 10^{-9} cm^2/s reported by Tung and Graham. Liu, Cohen, Adams, and Voter (1991) have thus re-fit the Tung and Graham (1980) data to an Arrhenius equation, assuming a preexponential factor of 0.001 cm^2/s. The reanalyzed Arrhenius parameters are shown in Table 3. The OJ, FBD, and VC models are in reasonable agreement with the reanalyzed experimental result for diffusion along the $[1\bar{1}0]$ direction. The reanalyzed diffusion rates, however, present discrepancies for diffusion along the [001] direction.

The first analysis of the Tung and Graham (1980) data (using $D_0 = 10^{-9}$ cm^2/s) suggests directional anisotropy in diffusion on the Ni(110) surface; reanalysis of the data ($D_0 = 10^{-3}$ cm^2/s) removes the

directional anisotropy of diffusion on the Ni(110) surface and suggest an activation energy of 0.45 eV for diffusion along both directions. Directional anisotropy on Ni(110), however, is clearly evident in the mass transfer results of Bonzel and Latta (1978). To confuse the issue further, directional anisotropy on Ni(110) is not evident in mass transfer studies by Maiya and Blakely (1965); in fact, no effect of surface orientation on diffusion rates is observed for the (100), (111), and (110) surfaces, leading Bonzel (1983) in his review to suggest that the nickel surfaces used in the study were insufficiently clean.

All four EAM models predict a directional anisotropy, and that adatom motion parallel to the channels is more probable than hopping between channels. This is clearly borne out in the Arrhenius plots (Figure 5) for the diffusion on (110) surface in $[1\bar{1}0]$ and [001] directions. Our calculated diffusion coefficients in the [001] direction are closer to the mass transfer results than the FIM data given by Tung and Graham (1980) or reanalyzed by Liu, Cohen, Adams, and Voter (1991); however, Bonzel (1983) suggests that because of the large preexponential factor attained from the mass transfer experiments, these Arrhenius parameters correspond to a nonlocalized diffusion process (which is by its nature isotropic), and, thus, the true diffusion rate in the [001] direction is not measured.

Diffusion across the channels on the (110) surface via adatom-exchange with one of the channel atoms has been observed (Wrigley and Ehrlich 1980). Additionally, there is evidence from the recent first-principles total-energy calculations that this complex mechanism for diffusion can be invoked for surface self-diffusion on the (100) surface (Kellog and Feibelman 1990). Liu, Cohen, Adams, and Voter (1991) calculate Arrhenius parameters for this atom exchange mechanism for diffusion across the channels on the Ni(110) surface, which are in reasonable agreement with the reanalyzed Tung and Graham (1980) data, and which predict a much lower activation energy (0.39 and 0.42 eV for VC and FBD-type models) for diffusion via adatom-exchange compared to our values (0.53 and 0.50 eV for VC and FBD models) based on hopping across the channels. The respective D_0's, 4.0 and 2.3×10^{-3} cm^2/s, are in agreement with our values, 3.8 and 3.3×10^{-3} cm^2/s.

Recently, Hansen, Stoltze, Jacobsen, and Nørskov (1991) examined diffusion on the (100) and (110) surfaces of copper via adatom-exchange and found that the energies calculated from the effective medium theory predict the adatom exchange mechanism as the energetically most favorable mechanism for diffusion on these surfaces. Furthermore, they found that a simple hopping mechanism is energetically favored for self-diffusion on (111) surface and in the [001] direction on the (110) surface. While these results thus indicate directional anisotropy in diffusion on the Cu(110) surface, there appears to be some

disagreement between their findings and Liu, Cohen, Adams, and Voter (1991) findings concerning the most energetically favorable mechanism for the Cu(100) surface as well. The latter studies based on VC and FBD-type EAM models show that Ni and Cu do not favor adatom exchange mechanism for diffusion on (100) surface and that self-diffusion on (110) surface, based on the exchange mechanism, is isotropic. Although we did not calculate rates of diffusion invoking this mechanism on either the (100) and (110) surfaces, our results, when compared to the Liu, Cohen, Adams, and Voter (1991) results, would suggest that the adatom exchange mechanism describes diffusion in the [001] direction on the (110) surface. Detailed MD studies (De Lorenzi, Jacucci, and Pontikis 1982) have shown that the predominance of the adatom exchange mechanism results in nearly isotropic diffusion which is further confirmed by recent calculations of Liu, Cohen, Adams, and Voter (1991) and that the superposition of all the other possible mechanisms leads to diffusion anisotropy on the (110) surface.

4. SUMMARY AND CONCLUSION

Calculations of Ni surface self-diffusion based upon VTST were performed using different EAM potentials in an effort to analyze their suitability in calculating surface and interfacial properties. In spite of the difficulty of comparing the calculated results with the measured values, the EAM potentials were successful in reproducing several observables of nickel adsorbed on its surfaces. On the basis of the hopping mechanism, all of the models predict the directional anisotropy for self-diffusion on the Ni(110) surface, that diffusion occurs more easily in the $[1\bar{1}0]$ direction, and that two distinct binding sites of Ni exist on the (111) surface. Estimated classical diffusion barriers indicate that diffusion occurs most easily on the (111) surface compared to other surfaces. At high temperatures, the models agree with each other; but as temperatures decrease, the predicted diffusivities fall within a scatterband as is clear from Figure 5.

Although all four embedded-atom pair functionals provide Arrhenius parameters which are in reasonable agreement with the measured experimental values for self-diffusion on Ni(100), the experimental differences in the rates of diffusion on the other surfaces must be resolved before a stringent comparison with the rates will indicate if further refinement is necessary for the EAM models. It is encouraging, however, that each of these models predict surface properties which have been determined, and predict reasonable behavior of diffusion on all of the surfaces. These studies involving the surface diffusivity and surface structure with realistic interaction potentials combined with recent advances in first-principles calculations as well as the explosive developments in the thin-film growth techniques should result in renewed impetus for more refined measurements of adatom diffusion.

5. REFERENCES

Ackland, G. J., G. Tichy, V. Vitek, and M. W. Finnis. Phil. Mag., vol. 56, p. 735, 1987.

Adams, J. B., S. M. Foiles, and W. G. Wolfer. J. Mater. Res., vol. 4, p. 102, 1989.

Bassett, D. W., and P. R. Webber. Surface Science, vol. 70, p. 520, 1978.

Bonzel, H. P. Surface Mobilities on Solid Materials, Fundamental Concepts and Applications. Edited by V. T. Binh, New York: Plenum, p. 230, 1983.

Bonzel, H. P., and E. E. Latta. Surface Science, vol. 76, p. 275, 1978.

Clementi, E., and C. Roetti. Atomic and Nuclear Data Tables. New York: Academic, vol. 14, nos. 3–4, 1974.

Daw, M. S., and M. I. Baskes. Phys. Rev. Lett., vol. 50, p. 1285, 1983.

Daw, M. S., and M. I. Baskes. Phys. Rev. B, vol. 29, p. 6443, 1984.

De Lorenzi, G. Computer Simulation in Physical Metallurgy. D. Reidel Publishing Company, G. Jacucci, editor, p. 43, 1986.

De Lorenzi, G., and G. Jacucci. Surface Science, vol. 164, p. 526, 1985.

De Lorenzi, G., G. Jacucci, and V. Pontikis. Surface Science, vol. 116, p. 391, 1982.

Doll, J. D., and A. F. Voter. Ann. Rev. Phys. Chem., vol. 38, p. 413, 1987.

Ehrlich, G. Scann. Micro., vol. 4, p. 829, 1990.

Ehrlich, G., and K. Stolt. Ann. Rev. Phys. Chem., vol. 31, p. 603, 1980.

Feibelman, P. J. Phys. Rev. Lett., vol. 65, p. 729, 1990.

Finnis, M. W., and J. Sinclair. Phil. Mag. A., vol. 50, p. 45, 1981.

Foiles, S. M. Phys. Rev. B, vol. 32, p. 3409, 1985.

Foiles, S. M. Surf. Sci. Lett., vol. 191, p. 779, 1987.

Foiles, S. M., M. I. Baskes, and M. S. Daw. Phys. Rev. B, vol. 33, p. 7983, 1986.

Halicioglu, T., and G. M. Pound. Thin Solid Films, vol. 57, p. 241, 1979.

Hansen, L., P. Stoltze, K. W. Jacobsen, and J. K. Nørskov. Phys. Rev. B, vol. 44, p. 6523, 1991.

Jacobsen, K. W., J. K. Nrskov, and M. J. Puska. Phys. Rev. B, vol. 35, p. 7423, 1987.

Johnson, R. A. Computer Simulation in Materials Science. Edited by R. J. Arsenault, J. Beeler, and D. M. Esterling, ASM, 1988.

Kellogg, G. L., and P. J. Feibelman. Phys. Rev. Lett., vol. 64, p. 3143, 1990.

Lauderdale, J. G., and D. G. Truhlar. Surface Science, vol. 164, p. 558, 1985.

Lee, J. K. (ed.) Interatomic Potentials and Crystalline Defects. New York: Metallurgical Society of AIME, 1981.

Liu, C. L., J. M. Cohen, J. B. Adams, and A. F. Voter. Surface Science, vol. 253, p. 334, 1991.

Maiya, P. S., and J. M. Blakely. Appl. Phys. Lett., vol. 7, p. 60, 1965.

Manninen, M. Phys. Rev. B, vol. 34, p. 8486, 1986.

Oh, D. J., and R. A. Johnson. Atomistic Simulation of Materials—Beyond Pair Potentials. Edited by V. Vitek and D. J. Srolovitz, New York: Plenum, 1989 and in J. Mater. Res., vol. 3, p. 471, 1988.

Rose, J. H., J. R. Smith, F. Guinea, and J. Ferrante. Phys. Rev. B, vol. 29, p. 2963, 1984.

Truhlar, D. G., A. D. Isaacson, and B. C. Garrett. Theory of Chemical Reaction Dynamics. Boca Raton, FL: CRC Press, vol 4, p. 65, 1983.

Truong, T. N., and D. G. Truhlar. J. Phys. Chem., vol. 91, p. 6229, 1987.

Truong, T. N., and D. G. Truhlar. J. Chem. Phys., vol. 88, p. 6611, 1988.

Tung, R. T., and W. R. Graham. Surface Science, vol. 97, p. 73, 1980.

Voter, A. F., and S. P. Chen. J. Mater. Res. Soc. Symp., vol. 82, p. 175, 1987.

Voter, A. F., and J. D. Doll. J. Chem. Phys., vol. 80, p. 5832, 1984.

Wrigley, J. D., and G. Ehrlich. Phys. Rev. Lett., vol. 44, p. 661, 1980.

LIST OF ACRONYMS

ATVF - Ackland, Tichy, Vitek, and Finnish model

BCC - body-centered cubic

EAM - embedded atom method

FBD - Foiles, Bashes, and Daw Model

FCC - face-centered cubic

FIM - field ion microscopy

MD - Molecular dynamic

OJ - Oh and Johnson model

VC - Voter and Chen model

VTST - variational transition state theory

INTENTIONALLY LEFT BLANK.

No. of Copies	Organization
2	Administrator Defense Technical Info Center ATTN: DTIC-DDA Cameron Station Alexandria, VA 22304-6145
1	Commander U.S. Army Materiel Command ATTN: AMCAM 5001 Eisenhower Ave. Alexandria, VA 22333-0001
1	Director U.S. Army Research Laboratory ATTN: AMSRL-D 2800 Powder Mill Rd. Adelphi, MD 20783-1145
1	Director U.S. Army Research Laboratory ATTN: AMSRL-OP-CI-A, Tech Publishing 2800 Powder Mill Rd. Adelphi, MD 20783-1145
2	Commander U.S. Army Armament Research, Development, and Engineering Center ATTN: SMCAR-IMI-I Picatinny Arsenal, NJ 07806-5000
2	Commander U.S. Army Armament Research, Development, and Engineering Center ATTN: SMCAR-TDC Picatinny Arsenal, NJ 07806-5000
1	Director Benet Weapons Laboratory U.S. Army Armament Research, Development, and Engineering Center ATTN: SMCAR-CCB-TL Watervliet, NY 12189-4050
(Unclass. only) 1	Commander U.S. Army Rock Island Arsenal ATTN: SMCRI-TL/Technical Library Rock Island, IL 61299-5000
1	Director U.S. Army Aviation Research and Technology Activity ATTN: SAVRT-R (Library) M/S 219-3 Ames Research Center Moffett Field, CA 94035-1000

No. of Copies	Organization
1	Commander U.S. Army Missile Command ATTN: AMSMI-RD-CS-R (DOC) Redstone Arsenal, AL 35898-5010
1	Commander U.S. Army Tank-Automotive Command ATTN: ASQNC-TAC-DIT (Technical Information Center) Warren, MI 48397-5000
1	Director U.S. Army TRADOC Analysis Command ATTN: ATRC-WSR White Sands Missile Range, NM 88002-5502
1	Commandant U.S. Army Field Artillery School ATTN: ATSF-CSI Ft. Sill, OK 73503-5000
(Class. only) 1	Commandant U.S. Army Infantry School ATTN: ATSH-CD (Security Mgr.) Fort Benning, GA 31905-5660
(Unclass. only) 1	Commandant U.S. Army Infantry School ATTN: ATSH-CD-CSO-OR Fort Benning, GA 31905-5660
1	WL/MNOI Eglin AFB, FL 32542-5000
	Aberdeen Proving Ground
2	Dir, USAMSAA ATTN: AMXSY-D AMXSY-MP, H. Cohen
1	Cdr, USATECOM ATTN: AMSTE-TC
1	Dir, ERDEC ATTN: SCBRD-RT
1	Cdr, CBDA ATTN: AMSCB-CI
1	Dir, USARL ATTN: AMSRL-SL-I
10	Dir, USARL ATTN: AMSRL-OP-CI-B (Tech Lib)

No. of Copies	Organization
1	HQDA (SARD-TC, C.H. Church) WASH DC 20310-0103
4	Commander US Army Research Office ATTN: R. Ghirardelli D. Mann R. Singleton R. Shaw P.O. Box 12211 Research Triangle Park, NC 27709-2211
2	Commander US Army Armament Research, Development, and Engineering Center ATTN: SMCAR-AEE-B, D.S. Downs SMCAR-AEE, J.A. Lannon Picatinny Arsenal, NJ 07806-5000
1	Commander US Army Armament Research, Development, and Engineering Center ATTN: SMCAR-AEE-BR, L. Harris Picatinny Arsenal, NJ 07806-5000
2	Commander US Army Missile Command ATTN: AMSMI-RD-PR-E, A.R. Maykut AMSMI-RD-PR-P, R. Betts Redstone Arsenal, AL 35898-5249
1	Office of Naval Research Department of the Navy ATTN: R.S. Miller, Code 432 800 N. Quincy Street Arlington, VA 22217
1	Commander Naval Air Systems Command ATTN: J. Ramnarace, AIR-54111C Washington, DC 20360
1	Commander Naval Surface Warfare Center ATTN: J.L. East, Jr., G-23 Dahlgren, VA 22448-5000
2	Commander Naval Surface Warfare Center ATTN: R. Bernecker, R-13 G.B. Wilmot, R-16 Silver Spring, MD 20903-5000

No. of Copies	Organization
5	Commander Naval Research Laboratory ATTN: M.C. Lin J. McDonald E. Oran J. Shnur R.J. Doyle, Code 6110 Washington, DC 20375
1	Commanding Officer Naval Underwater Systems Center Weapons Dept. ATTN: R.S. Lazar/Code 36301 Newport, RI 02840
2	Commander Naval Weapons Center ATTN: T. Boggs, Code 388 T. Parr, Code 3895 China Lake, CA 93555-6001
1	Superintendent Naval Postgraduate School Dept. of Aeronautics ATTN: D.W. Netzer Monterey, CA 93940
3	AL/LSCF ATTN: R. Corley R. Geisler J. Levine Edwards AFB, CA 93523-5000
1	AFOSR ATTN: J.M. Tishkoff Bolling Air Force Base Washington, DC 20332
1	OSD/SDIO/IST ATTN: L. Caveny Pentagon Washington, DC 20301-7100
1	Commandant USAFAS ATTN: ATSF-TSM-CN Fort Sill, OK 73503-5600
1	F.J. Seiler ATTN: S.A. Shackleford USAF Academy, CO 80840-6528

No. of Copies	Organization
1	University of Dayton Research Institute ATTN: D. Campbell AL/PAP Edwards AFB, CA 93523
1	NASA Langley Research Center Langley Station ATTN: G.B. Northam/MS 168 Hampton, VA 23365
4	National Bureau of Standards ATTN: J. Hastie M. Jacox T. Kashiwagi H. Semerjian US Department of Commerce Washington, DC 20234
1	Applied Combustion Technology, Inc. ATTN: A.M. Varney P.O. Box 607885 Orlando, FL 32860
2	Applied Mechanics Reviews The American Society of Mechanical Engineers ATTN: R.E. White A.B. Wenzel 345 E. 47th Street New York, NY 10017
1	Atlantic Research Corp. ATTN: R.H.W. Waesche 7511 Wellington Road Gainesville, VA 22065
1	AVCO Everett Research Laboratory Division ATTN: D. Stickler 2385 Revere Beach Parkway Everett, MA 02149
1	Battelle ATTN: TACTEC Library, J. Huggins 505 King Avenue Columbus, OH 43201-2693
1	Cohen Professional Services ATTN: N.S. Cohen 141 Channing Street Redlands, CA 92373

No. of Copies	Organization
1	Exxon Research & Eng. Co. ATTN: A. Dean Route 22E Annandale, NJ 08801
1	General Applied Science Laboratories, Inc. 77 Raynor Avenue Ronkonkama, NY 11779-6649
1	General Electric Ordnance Systems ATTN: J. Mandzy 100 Plastics Avenue Pittsfield, MA 01203
1	General Motors Rsch Labs Physical Chemistry Department ATTN: T. Sloane Warren, MI 48090-9055
2	Hercules, Inc. Allegheny Ballistics Lab. ATTN: W.B. Walkup E.A. Yount P.O. Box 210 Rocket Center, WV 26726
1	Alliant Techsystems, Inc. Marine Systems Group ATTN: D.E. Broden/MS MN50-2000 600 2nd Street NE Hopkins, MN 55343
1	Alliant Techsystems, Inc. ATTN: R.E. Tompkins 7225 Northland Drive Brooklyn Park, MN 55428
1	IBM Corporation ATTN: A.C. Tam Research Division 5600 Cottle Road San Jose, CA 95193
1	IIT Research Institute ATTN: R.F. Remaly 10 West 35th Street Chicago, IL 60616

No. of Copies	Organization
2	Director Lawrence Livermore National Laboratory ATTN: C. Westbrook M. Costantino P.O. Box 808 Livermore, CA 94550
1	Lockheed Missiles & Space Co. ATTN: George Lo 3251 Hanover Street Dept. 52-35/B204/2 Palo Alto, CA 94304
1	Director Los Alamos National Lab ATTN: B. Nichols, T7, MS-B284 P.O. Box 1663 Los Alamos, NM 87545
1	National Science Foundation ATTN: A.B. Harvey Washington, DC 20550
1	Olin Ordnance ATTN: V. McDonald, Library P.O. Box 222 St. Marks, FL 32355-0222
1	Paul Gough Associates, Inc. ATTN: P.S. Gough 1048 South Street Portsmouth, NH 03801-5423
2	Princeton Combustion Research Laboratories, Inc. ATTN: N.A. Messina M. Summerfield Princeton Corporate Plaza Bldg. IV, Suite 119 11 Deerpark Drive Monmouth Junction, NJ 08852
1	Hughes Aircraft Company ATTN: T.E. Ward 8433 Fallbrook Avenue Canoga Park, CA 91303

No. of Copies	Organization
1	Rockwell International Corp. Rocketdyne Division ATTN: J.E. Flanagan/HB02 6633 Canoga Avenue Canoga Park, CA 91304
4	Director Sandia National Laboratories Division 8354 ATTN: R. Cattolica S. Johnston P. Mattern D. Stephenson Livermore, CA 94550
1	Science Applications, Inc. ATTN: R.B. Edelman 23146 Cumorah Crest Woodland Hills, CA 91364
3	SRI International ATTN: G. Smith D. Crosley D. Golden 333 Ravenswood Avenue Menlo Park, CA 94025
1	Stevens Institute of Tech. Davidson Laboratory ATTN: R. McAlevy, III Hoboken, NJ 07030
1	Sverdrup Technology, Inc. LERC Group ATTN: R.J. Locke, MS SVR-2 2001 Aerospace Parkway Brook Park, OH 44142
1	Sverdrup Technology, Inc. ATTN: J. Deur 2001 Aerospace Parkway Brook Park, OH 44142
1	Thiokol Corporation Elkton Division ATTN: S.F. Palopoli P.O. Box 241 Elkton, MD 21921

No. of Copies	Organization
3	Thiokol Corporation Wasatch Division ATTN: S.J. Bennett P.O. Box 524 Brigham City, UT 84302
1	United Technologies Research Center ATTN: A.C. Eckbreth East Hartford, CT 06108
1	United Technologies Corp. Chemical Systems Division ATTN: R.R. Miller P.O. Box 49028 San Jose, CA 95161-9028
1	Universal Propulsion Company ATTN: H.J. McSpadden 25401 North Central Avenue Phoenix, AZ 85027-7837
1	Veritay Technology, Inc. ATTN: E.B. Fisher 4845 Millersport Highway P.O. Box 305 East Amherst, NY 14051-0305
1	Brigham Young University Dept. of Chemical Engineering ATTN: M.W. Beckstead Provo, UT 84058
1	California Institute of Tech. Jet Propulsion Laboratory ATTN: L. Strand/MS 125-224 4800 Oak Grove Drive Pasadena, CA 91109
1	California Institute of Technology ATTN: F.E.C. Culick/MC 301-46 204 Karman Lab. Pasadena, CA 91125
1	University of California Los Alamos Scientific Lab. P.O. Box 1663, Mail Stop B216 Los Alamos, NM 87545
1	University of California, Berkeley Chemistry Deparment ATTN: C. Bradley Moore 211 Lewis Hall Berkeley, CA 94720
1	University of California, San Diego ATTN: F.A. Williams AMES, B010 La Jolla, CA 92093
2	University of California, Santa Barbara Quantum Institute ATTN: K. Schofield M. Steinberg Santa Barbara, CA 93106
1	University of Colorado at Boulder Engineering Center ATTN: J. Daily Campus Box 427 Boulder, CO 80309-0427
2	University of Southern California Dept. of Chemistry ATTN: S. Benson C. Wittig Los Angeles, CA 90007
1	Cornell University Department of Chemistry ATTN: T.A. Cool Baker Laboratory Ithaca, NY 14853
1	University of Delaware ATTN: T. Brill Chemistry Department Newark, DE 19711
1	University of Florida Dept. of Chemistry ATTN: J. Winefordner Gainesville, FL 32611
3	Georgia Institute of Technology School of Aerospace Engineering ATTN: E. Price W.C. Strahle B.T. Zinn Atlanta, GA 30332

No. of Copies	Organization
1	University of Illinois Dept. of Mech. Eng. ATTN: H. Krier 144MEB, 1206 W. Green St. Urbana, IL 61801
1	The Johns Hopkins University Chemical Propulsion Information Agency ATTN: T.W. Christian 10630 Little Patuxent Parkway, Suite 202 Columbia, MD 21044-3200
1	University of Michigan Gas Dynamics Lab Aerospace Engineering Bldg. ATTN: G.M. Faeth Ann Arbor, MI 48109-2140
1	University of Minnesota Dept. of Mechanical Engineering ATTN: E. Fletcher Minneapolis, MN 55455
3	Pennsylvania State University Applied Research Laboratory ATTN: K.K. Kuo H. Palmer M. Micci University Park, PA 16802
1	Pennsylvania State University Dept. of Mechanical Engineering ATTN: V. Yang University Park, PA 16802
1	Polytechnic Institute of NY Graduate Center ATTN: S. Lederman Route 110 Farmingdale, NY 11735
2	Princeton University Forrestal Campus Library ATTN: K. Brezinsky I. Glassman P.O. Box 710 Princeton, NJ 08540
1	Purdue University School of Aeronautics and Astronautics ATTN: J.R. Osborn Grissom Hall West Lafayette, IN 47906
1	Purdue University Department of Chemistry ATTN: E. Grant West Lafayette, IN 47906
2	Purdue University School of Mechanical Engineering ATTN: N.M. Laurendeau S.N.B. Murthy TSPC Chaffee Hall West Lafayette, IN 47906
1	Rensselaer Polytechnic Inst. Dept. of Chemical Engineering ATTN: A. Fontijn Troy, NY 12181
1	Stanford University Dept. of Mechanical Engineering ATTN: R. Hanson Stanford, CA 94305
1	University of Texas Dept. of Chemistry ATTN: W. Gardiner Austin, TX 78712
1	Virginia Polytechnic Institute and State University ATTN: J.A. Schetz Blacksburg, VA 24061
1	Freedman Associates ATTN: E. Freedman 2411 Diana Road Baltimore, MD 21209-1525

USER EVALUATION SHEET/CHANGE OF ADDRESS

This Laboratory undertakes a continuing effort to improve the quality of the reports it publishes. Your comments/answers to the items/questions below will aid us in our efforts.

1. ARL Report Number ARL-TR-5 Date of Report November 1992

2. Date Report Received _____

3. Does this report satisfy a need? (Comment on purpose, related project, or other area of interest for which the report will be used.) _____

4. Specifically, how is the report being used? (Information source, design data, procedure, source of ideas, etc.) _____

5. Has the information in this report led to any quantitative savings as far as man-hours or dollars saved, operating costs avoided, or efficiencies achieved, etc? If so, please elaborate. _____

6. General Comments. What do you think should be changed to improve future reports? (Indicate changes to organization, technical content, format, etc.) _____

CURRENT ADDRESS

_____
Organization

_____
Name

_____
Street or P.O. Box No.

_____
City, State, Zip Code

7. If indicating a Change of Address or Address Correction, please provide the Current or Correct address above and the Old or Incorrect address below.

OLD ADDRESS

_____
Organization

_____
Name

_____
Street or P.O. Box No.

_____
City, State, Zip Code

(Remove this sheet, fold as indicated, staple or tape closed, and mail.)

DEPARTMENT OF THE ARMY

OFFICIAL BUSINESS

BUSINESS REPLY MAIL
FIRST CLASS PERMIT No 0001, APG, MD

Postage will be paid by addressee

Director
U.S. Army Research Laboratory
ATTN: AMSRL-OP-CI-B (Tech Lib)
Aberdeen Proving Ground, MD 21005-5066

NO POSTAGE
NECESSARY
IF MAILED
IN THE
UNITED STATES